

AD-A201 548

DTIC FILE COPY.

AD E 951221

(2)

TECHNICAL REPORT RD-ST-88-1

ANALYSIS OF PERSHING II REENTRY VEHICLE (RV)
CONTROL RING CASTINGS

Albert S. Ingram
Structures Directorate
Research, Development, and Engineering Center

MAY 1988



U.S. ARMY MISSILE COMMAND

Redstone Arsenal, Alabama 35898-5000

Approved for public release; distribution is unlimited.

DTIC
ELECTED
DEC 19 1988
S C H D

58 12 19 094

DISPOSITION INSTRUCTIONS

**DESTROY THIS REPORT WHEN IT IS NO LONGER NEEDED. DO NOT
RETURN IT TO THE ORIGINATOR.**

DISCLAIMER

**THE FINDINGS IN THIS REPORT ARE NOT TO BE CONSTRUED AS AN
OFFICIAL DEPARTMENT OF THE ARMY POSITION UNLESS SO DESIGN-
NATED BY OTHER AUTHORIZED DOCUMENTS.**

TRADE NAMES

**USE OF TRADE NAMES OR MANUFACTURERS IN THIS REPORT DOES
NOT CONSTITUTE AN OFFICIAL ENDORSEMENT OR APPROVAL OF
THE USE OF SUCH COMMERCIAL HARDWARE OR SOFTWARE.**

UNCLASSIFIED

SECURITY CLASSIFICATION OF THIS PAGE

REPORT DOCUMENTATION PAGE				Form Approved OMB No 0704-0188 Exp. Date Jun 30, 1986												
1a. REPORT SECURITY CLASSIFICATION UNCLASSIFIED		1b. RESTRICTIVE MARKINGS														
2a. SECURITY CLASSIFICATION AUTHORITY		3. DISTRIBUTION/AVAILABILITY OF REPORT Approved for public release; distribution is unlimited.														
2b. DECLASSIFICATION/DOWNGRADING SCHEDULE																
4. PERFORMING ORGANIZATION REPORT NUMBER(S) RD-ST-88-1		5. MONITORING ORGANIZATION REPORT NUMBER(S)														
6a. NAME OF PERFORMING ORGANIZATION Structures Directorate, Res. Dev. and Engr Ctr	6b. OFFICE SYMBOL (If applicable) AMSMI-RD-ST	7a. NAME OF MONITORING ORGANIZATION														
6c. ADDRESS (City, State, and ZIP Code) Commander U. S. Army Missile Command ATTN: AMSMI-RD-ST Redstone Arsenal, AL 35898-5247		7b. ADDRESS (City, State, and ZIP Code)														
8a. NAME OF FUNDING/SPONSORING ORGANIZATION	8b. OFFICE SYMBOL (If applicable)	9. PROCUREMENT INSTRUMENT IDENTIFICATION NUMBER														
8c. ADDRESS (City, State, and ZIP Code)		10. SOURCE OF FUNDING NUMBERS <table border="1"><tr><td>PROGRAM ELEMENT NO.</td><td>PROJECT NO.</td><td>TASK NO.</td><td>WORK UNIT ACCESSION NO</td></tr></table>			PROGRAM ELEMENT NO.	PROJECT NO.	TASK NO.	WORK UNIT ACCESSION NO								
PROGRAM ELEMENT NO.	PROJECT NO.	TASK NO.	WORK UNIT ACCESSION NO													
11. TITLE (Include Security Classification) Analysis of PERSHING II Reentry Vehicle Control Ring Castings																
12. PERSONAL AUTHOR(S) Albert S. Ingram																
13a. TYPE OF REPORT Technical	13b. TIME COVERED FROM Mar 87 TO Aug 87	14. DATE OF REPORT (Year, Month, Day) MAY 1988	15. PAGE COUNT 34													
16. SUPPLEMENTARY NOTATION																
17. COSATI CODES <table border="1"><tr><th>FIELD</th><th>GROUP</th><th>SUB-GROUP</th></tr><tr><td></td><td></td><td></td></tr><tr><td></td><td></td><td></td></tr><tr><td></td><td></td><td></td></tr></table>		FIELD	GROUP	SUB-GROUP										18. SUBJECT TERMS (Continue on reverse if necessary and identify by block number) A356 aluminum, elongation, eutectic silicon, fracture toughness, tensile strength, (Ingram) K _{IC}		
FIELD	GROUP	SUB-GROUP														
19. ABSTRACT (Continue on reverse if necessary and identify by block number) A comparative material analysis was performed on two PERSHING II RV control rings with reported differences in tensile properties and percent elongation. Both RV control rings were characterized by tensile tests, chemical analysis, fracture toughness tests, and metallography. The comparative analysis proved that the two examined RV rings were equivalent, though contractor tensile coupon tests showed otherwise. The average properties of the RV control ring were; 37.25 ksi (256.6 MPa) ultimate strength, 32.65 ksi (225 MPa) yield strength, 5.7 percent elongation, and 15.505 ksi ^{in.} (16.55 MPa ^M) K _{IC} fracture toughness. The RV rings are fabricated from A356-T6 aluminum. Sq. root																
20. DISTRIBUTION/AVAILABILITY OF ABSTRACT <input type="checkbox"/> UNCLASSIFIED/UNLIMITED <input checked="" type="checkbox"/> SAME AS RPT. <input type="checkbox"/> DTIC USERS		21. ABSTRACT SECURITY CLASSIFICATION UNCLASSIFIED														
22a. NAME OF RESPONSIBLE INDIVIDUAL Albert S. Ingram		22b. TELEPHONE (Include Area Code) (205) 876-2742	22c. OFFICE SYMBOL AMSMI-RD-ST													

TABLE OF CONTENTS

	<u>Page</u>
I. INTRODUCTION.....	1
II. APPROACH.....	1
III. EXPERIMENTAL RESULTS.....	4
A. Mechanical Property Tests - RV Control Rings.....	4
B. Microstructural Examination - RV Control Rings.....	12
C. Fractography - RV Control Rings.....	12
D. Chemical Analysis - RV Control Rings.....	12
E. Analysis of Hemet Tensile Coupons.....	15
IV. CONCLUSIONS.....	24
V. RECOMMENDATIONS.....	24
REFERENCES.....	25



Accession For	
NTIS GRA&I	<input checked="" type="checkbox"/>
DTIC TAB	<input type="checkbox"/>
Unannounced	<input type="checkbox"/>
Justification	
By _____	
Distribution/ _____	
Availability Codes	
Dist	Avail and/or Special
A-1	

LIST OF ILLUSTRATIONS

<u>Figure</u>		<u>Page</u>
1	Side view of a PII RV control ring.....	2
2	Top view of a PII RV control ring. Note the four jet vane ports (1) and the four web sections (2).....	3
3	Tensile specimen. RV control ring casting.....	5
4	Fracture toughness specimen.....	9
5	Typical fracture toughness specimen used in this analysis (2.5X).....	10
6	Photograph of fracture surface of typical fracture toughness specimen. Note fatigue pre-crack zone (1) and flat, fast fracture zone (2) (1.1X).....	10
7	Typical microstructure found in the jet vane port section of each RV control ring. Note the size and shape of the eutectic silicon phase. Keller's ETCH (100X).....	13
8	Typical microstructure found in the web section of each RV control ring. Compare with Figure 7 (100X).....	13
9	Typical fracture morphology in fatigue zone of fracture toughness samples. Fatigue cracking has occurred along favorably oriented eutectic silicon particles (100X).....	14
10	Typical fracture morphology of tensile overload. This was found in tensile test samples and the fast fracture zone of fracture toughness specimens. Compare with Figure 9 (100X).....	14
11	Stairstep type fatigue striations found in fatigue zone of fracture toughness specimen (620X).....	17
12	Macrograph of tensile coupon fracture showing extensive casting flaws (11.5X).....	17
13	Scanning electron micrograph of typical casting flaws. Note the distinct irregular appearance (28X).....	18
14	High magnification SEM photograph of casting flaw showing uneven ridges which are believed to be the tips of dendrite tree networks (500X).....	18
15	Typical Group 1 fracture surface away from casting flaws. Compare with Figure 16 (300X).....	19
16	Typical Group 2 fracture surface. Fracture morphology is generally less coarse than that in Group 1 (300X).....	19

LIST OF ILLUSTRATIONS (Concluded)

<u>Figure</u>		<u>Page</u>
17	Typical microporosity which was found in all examined samples of Group 1 and Group 2 (100X).....	20
18	Polished and etched cross section of a Group 1 tensile coupon. Note the dense network of eutectic silicon and dendrites at the break.....	20
19	Magnified view of Figure 18 showing fracture occurring along the network of segregated eutectic silicon (35X).....	21
20	Microstructure of Group 2 tensile coupon having 6 percent elongation. Compare to Figure 21 (100X).....	21
21	Microstructure of Group 2 tensile coupon with 10 percent elongation. Compare to Figure 20 (100X).....	22

LIST OF TABLES

<u>Tables</u>		<u>Page</u>
1 RV Ring SN 60428 Tensile Property Tests.....		6
2 RV Ring SN 10253 Tensile Property Tests.....		7
3 Fracture Toughness Tests.....		11
4 Chemical Analysis RV Control Rings.....		15
5 Chemical Analysis RV Control Rings.....		23

ACKNOWLEDGMENT

The professional efforts of the following individuals are gratefully acknowledged:

Eugene L. Goodwin, U.S. Army Missile Command, Metallography
Steven Carr, U.S. Army Missile Command, Chemical Analysis
Alexis Von Spakovsky, U.S. Army Missile Command, Computer Assistance
Richard Busch, Sperry Corporation, Computer Analysis
Marcus Thomas, Sperry Corporation, Mechanical Testing

I. INTRODUCTION

Structures Directorate, Composite Structures and Materials Function, performed a material analysis on the PERSHING II (PII) Reentry Vehicle (RV) control ring casting, APN 11502352-3. Basically, the objective of the analysis was to evaluate RV control rings with reported low mechanical properties. The RV control ring is manufactured by Hemet Casting Company, Hemet, CA. Due to the falsification of Hemet quality control tensile tests data between 1982 and 1985, approximately 55 RV control rings with below specification tensile properties were issued Certificates of Compliance and allowed to be installed into PII missile assemblies. Martin Marietta Corporation performed a study of these falsified tensile test data [1] and reported corrected tensile properties of some RV control rings as low as 31.4 ksi (216 MPa) ultimate strength, 22.9 ksi (158 MPa) yield strength, and 1 percent elongation. The RV control ring is specified to be fabricated from A356, Class 10 aluminum casting alloy per MIL-A-21180. After appropriate solution heat treatment and artificial aging (A356-T6), the RV control ring is required to have the minimum tensile properties of 38 ksi (262 MPa) ultimate strength, 28 ksi (193 MPa) yield strength, and 5 percent elongation. A RV control ring is shown in Figures 1 and 2.

II. APPROACH

Of major concern in this analysis was the lack of ductility (low percent elongation) which was documented for several RV control ring castings. It was shown in [1] that RV rings with reduced mechanical properties of yield and ultimate strength were still capable of performing their intended mission. However, elongation is a property which indicates the toughness of the material. Since the RV control ring is an aluminum casting with inherent lower toughness and percent elongation than wrought aluminum alloys of the same strength level, a serious loss of toughness would make the RV ring less tolerant of stress risers, flaws, and random, unexpected loads. Therefore, to quantify the loss of properties which could occur from below specification strength and elongation properties, a comparative analysis was performed on two RV control rings, i.e., one RV ring with proper percent elongation and one RV ring with below specification percent elongation. The received RV control rings had the following reported properties:

	<u>SN/10253 /</u>	<u>SN 60428 *</u>
ultimate strength	37.7 ksi (232.4 MPa)	38 ksi (262 MPa)
yield strength	29.3 ksi (202 MPa)	28 ksi (193 MPa)
% elongation x	2.5	5

/ As reported properties per [1]

* As reported properties per Certificate of Compliance

x 1 in. gage length used, 0.250 in. diameter tensile coupons

The comparative analysis consisted of the following:

- A. Mechanical Property Tests
- B. Fracture Toughness Tests
- C. Critical Flaw Size Analysis
- D. Microstructural Examination
- E. Fractography

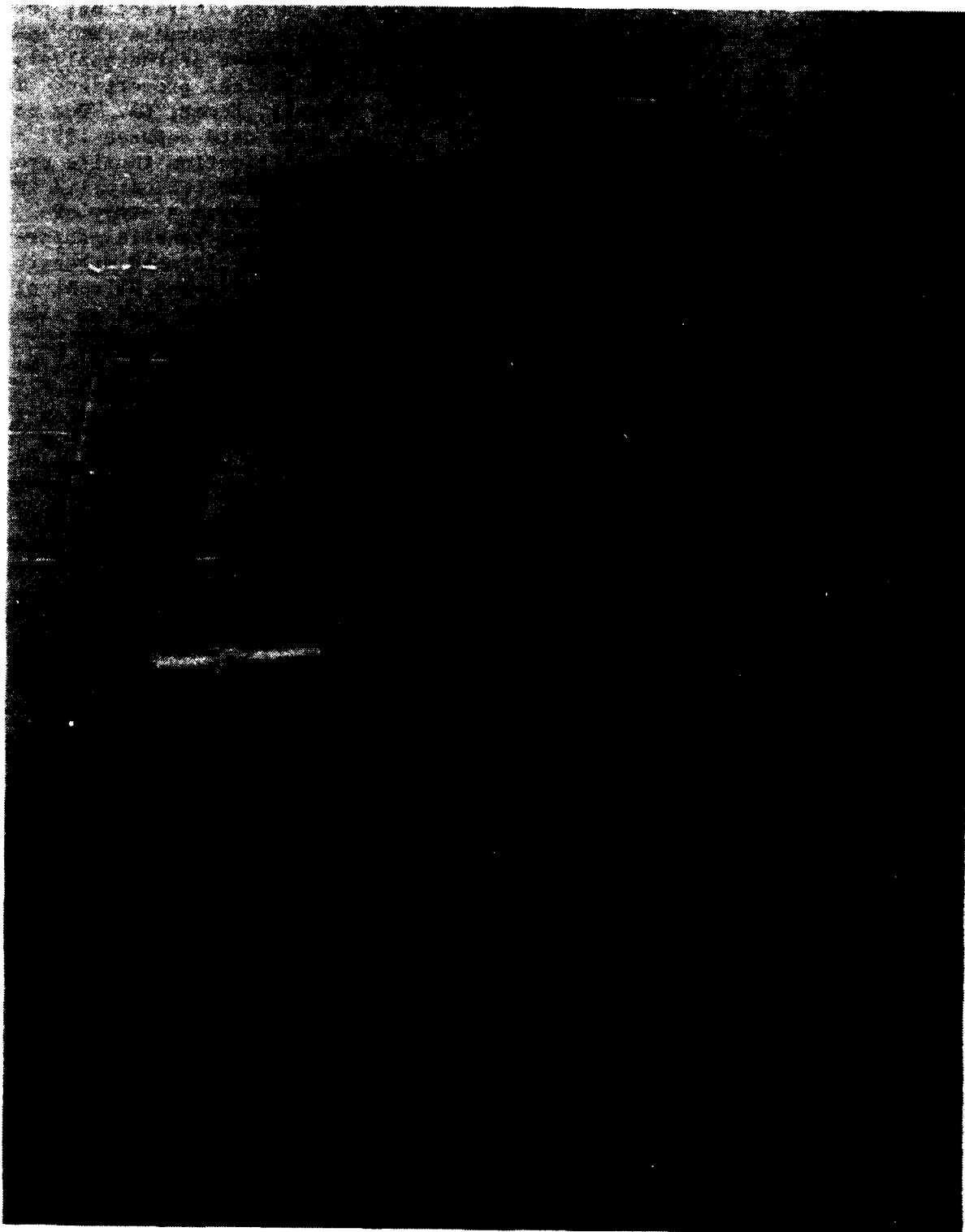


Figure 1. Side view of a PII RV control ring.

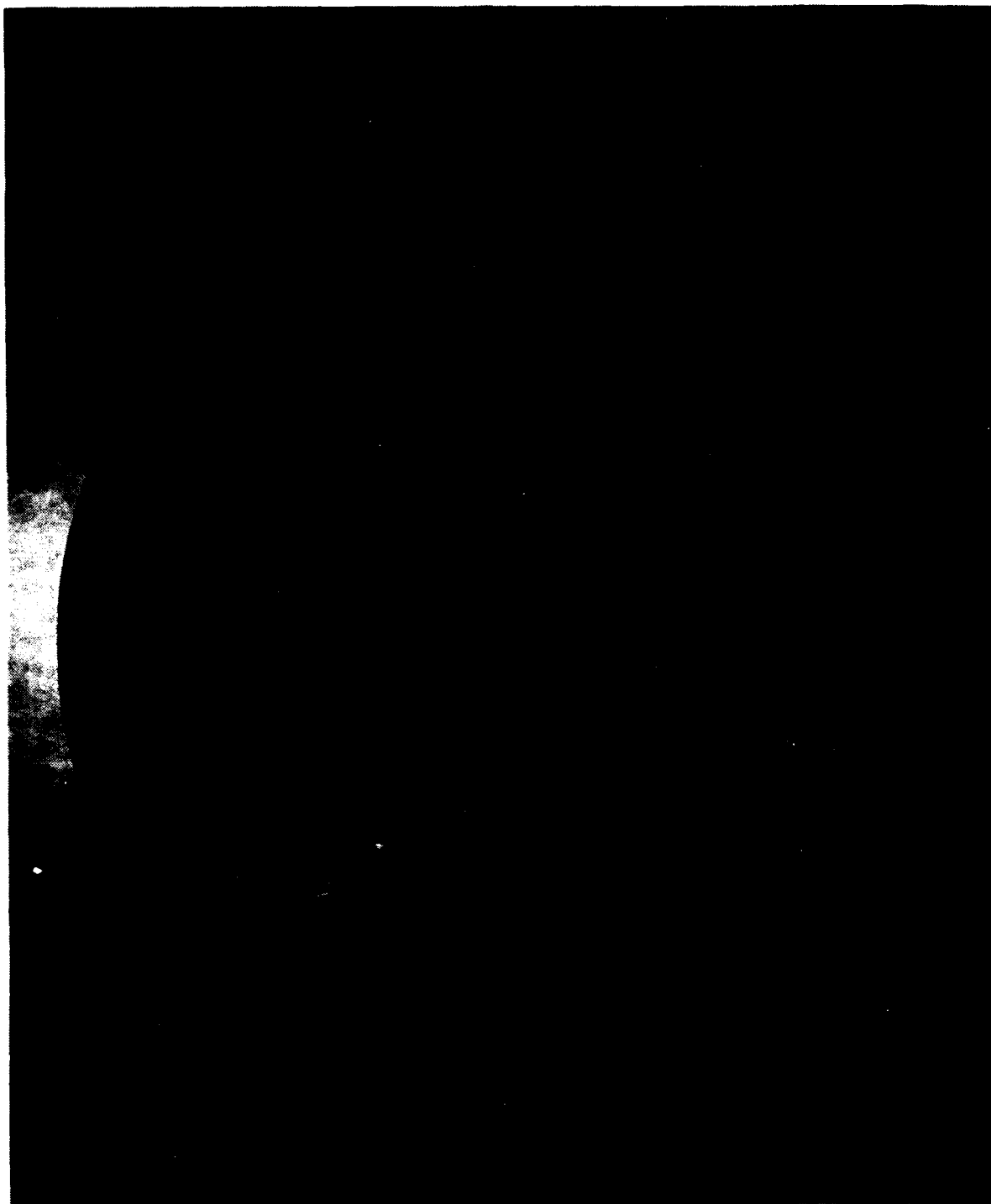


Figure 2. Top view of a PII RV control ring. Note the four jet vane ports (1) and the four web sections (2).

Additionally, 179 broken tensile coupons from Hemet Casting Company were received for analysis. These samples were a portion of the actual tensile test coupons used for mechanical property evaluation (quality control) of the RV control rings. An analysis was performed to determine the major differences between tensile coupons with low and high percent elongation.

III. EXPERIMENTAL RESULTS

A. Mechanical Property Tests - RV Control Rings

1. Tensile Tests

To establish the nominal tensile strength properties of each RV control ring, twelve tensile specimens were fabricated from the web sections of each RV control ring, Figures 2 and 3. Though the web section has a nominal thickness of only 0.10 in. (2.54 mm), it was judged to be the best available area for tensile specimens since the thicker jet vane port sections were allocated for fracture toughness specimens. No significant differences in tensile properties or percent elongation were found between the two RV control rings. Neither RV ring had an average ultimate strength equal to the required 38 ksi (262 Mpa) level. Results are shown in Tables 1 and 2.

2. Stress Concentration Tests

To evaluate the effect of stress risers on the ultimate tensile strength of each RV ring, stress concentration tensile tests were performed. The stress concentration specimen was identical to the 2 in. gage length tensile specimens (Figure 3) except a 0.062-in. (1.6 mm) diameter hole was drilled (through thickness) at the center of the gage length. In theory, a stress concentration factor as high as 3.00 could be produced at a small hole in a stressed plate of infinite width [2]. Therefore, when subjected to high stress concentrations, a brittle material would be expected to fail at a lower ultimate tensile strength than would occur if tested in a standard or normal tensile test. Eight stress concentration specimens were tested from each RV control ring. No significant differences were found. Results are shown in Tables 1 and 2.

3. Percent Elongation

Since all previous reported elongation data for the RV control rings has been generated from 1 in. gage length tensile samples, gage marks of 1 in. (25.4 mm) and 2 in. (50.8 mm) lengths were placed on all tensile samples and stress concentration samples. This would allow these results to be compared with existing 1 in. gage length percent elongation data. In addition, the elongation of the stress concentration tests is reported as a comparative value and is intended to reflect the degree of ductility resulting from this particular test only. No significant differences in elongation were found between RV control rings SN 10253 and SN 60428. RV ring SN 10253 had an average elongation of 5.4 percent; not 2.5 percent as indicated by Hemet tensile coupon tests.

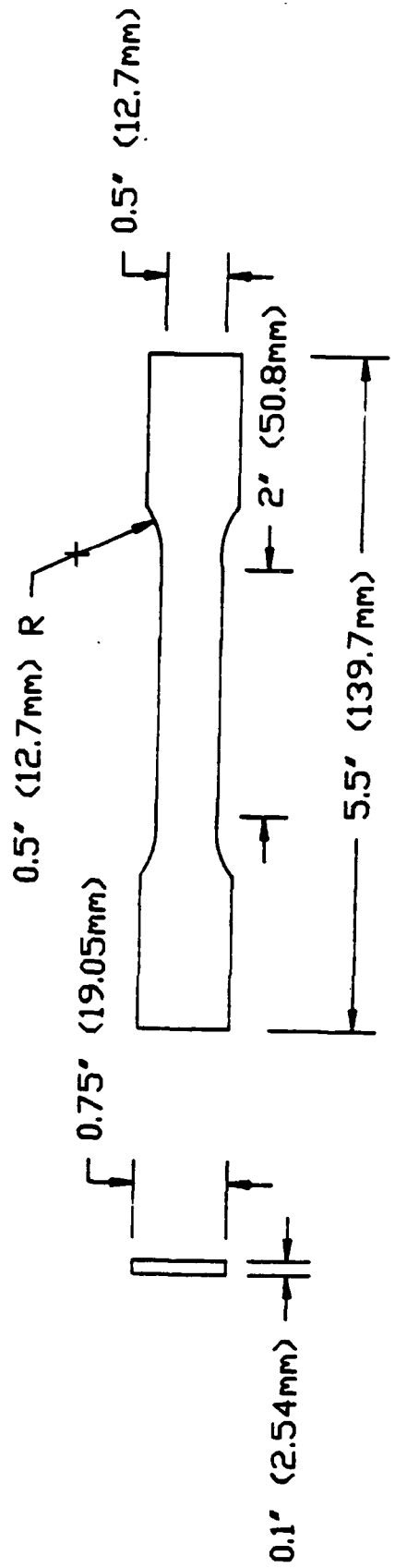


Figure 3. Tensile specimen. RV control ring casting.

TABLE 1. RV Ring SN 60428 Tensile Property Tests.

SECTION-SPECIMEN	YIELD STRENGTH KSI (MPA)	ULTIMATE STRENGTH KSI (MPA)	% Elongation 2 in. (50.8mm) Gage Length		% Elongation 1 in. (25.4mm) Gage Length	
			4:1	4:3	4:1	4:3
1-1	34.9 {240.4}	38.1 {263.0}			2.2	5.0
1-2	32.8 {226.1}	35.8 {246.8}			2.0	
1-3	30.5 {210.5}	36.5 {251.8}			2.5	
1-4 *	NA	38.7 {266.5}			1.0	
1-5 *	NA	36.6 {252.0}			1.5	
2-1	33.2 {229.1}	37.5 {258.6}			2.5	
2-2	34.3 {236.4}	37.7 {259.6}			2.0	5.5
2-3	32.9 {227.1}	38.3 {264.2}			4.0	/
2-4 *	NA	38.0 {261.7}			1.0	4.1
2-5 *	NA	33.7 {232.3}			1.0	4.0
3-1	32.3 {222.8}	36.5 {261.4}			3.0	
3-2	34.0 {234.6}	38.0 {262.2}			3.5	5.9
3-3	33.1 {228.3}	38.9 {268.5}			4.0	7.2
3-4 *	NA	36.0 {248.0}			1.0	4.6
3-5 *	NA	36.7 {253.0}			1.0	3.8
4-1	34.3 {236.5}	37.0 {254.8}			1.5	
4-2	34.8 {240.0}	38.1 {262.4}			✓	5.2
4-3	32.9 {227.1}	38.3 {264.4}			4.0	
4-4 *	NA	36.4 {251.1}			1.0	6.3
4-5 *	NA	38.5 {265.1}			1.5	* Stress Concentration Specimen

Tensile Tests - Average Results

Ultimate Strength, KSI (MPa) = 37.6 (259.0)
 Yield Strength, KSI (MPa) = 33.3 (229.9)
 Elongation, 1 in. (25.4mm) Gage Length = 5.9%
 Elongation, 2 in. (50.8mm) Gage Length = 2.8%

Stress Concentration Test - Average Results

Ultimate Strength, KSI (MPa) = 36.8 (253.7)
 Elongation, 1 in. (25.5mm) Gage Length = 4.3%
 Elongation, 2 in. (50.8mm) Gage Length = 1.1%

TABLE 2. RV Ring SN 10253 Tensile Property Tests.

SECTION-SPECIMEN	YIELD STRENGTH KSI (MPa)	ULTIMATE STRENGTH KSI (MPa)	% Elongation 2 in. (50.8 mm) Gage Length		% Elongation 1 in. (25.4 mm) Gage Length
			% Elongation 2 in. (50.8 mm) Gage Length	% Elongation 1 in. (25.4 mm) Gage Length	
1-1	32.6 (224.6)	37.6 (259.1)	2.2	5.5	
1-2	31.9 (220.2)	36.4 (251.1)	2.3	5.4	
1-3	32.1 (221.1)	36.6 (252.2)	2.0	5.0	
1-4 *	NA	37.4 (257.8)	1.5	4.5	
1-5 *	NA	35.7 (250.0)	1.8	4.0	
2-1	31.3 (215.5)	36.5 (251.5)	2.0	5.3	
2-2	32.2 (222.0)	36.9 (254.8)	✓		
2-3	31.8 (219.2)	36.6 (252.6)	2.8	5.4	
2-4 *	NA	35.9 (247.5)	1.5	4.1	
2-5 *	NA	36.5 (251.9)	1.5	3.5	
3-1	32.6 (225.1)	36.4 (250.7)	2.5	5.8	
3-2	33.1 (228.5)	37.7 (259.6)	2.5	4.9	
3-3	31.3 (215.6)	36.4 (250.7)	3.3	5.9	
3-4 *	NA	37.7 (259.8)	1.5	4.5	
3-5 *	NA	36.2 (249.6)	1.6	4.7 ✓ Broke outside	
4-1	33.0 (227.2)	36.0 (248.0)	2.0	5.5	Gage Length
4-2	30.2 (208.5)	37.3 (257.3)	2.5	5.1	
4-3	31.4 (216.3)	38.1 (262.9)	2.8	6.0 *	Stress
4-4 *	NA	35.1 (242.1)	1.8	4.1	Concentration
4-5 *	NA	36.7 (253.1)	2.0	4.0	Specimen

Tensile Tests - Average Results

Ultimate Strength, KSI (MPa) = 36.9 (254.2)
 Yield Strength, KSI (MPa) = 32.0 (220.3)
 Elongation, 1 in. (25.4 mm) Gage Length = 5.4%
 Elongation, 2 in. (50.8 mm) Gage Length = 2.5%

Stress Concentration Test - Average Results

Ultimate Strength, KSI (MPa) = 36.4 (251.0)
 Elongation, 1 in. (25.4 mm) Gage Length = 4.2%
 Elongation, 2 in. (50.8 mm) Gage Length = 1.7%

4. Fracture Toughness Tests

In order to adequately characterize the toughness of the two RV control rings, fracture toughness specimens (Figure 4) were fabricated from the thickest sections around the jet vane ports. A total of 14 specimens were tested; 8 from RV ring SN 60428 and 6 from RV ring SN 10253. ASTM E399 test methods for K_{IC} fracture toughness determination were followed. A typical fracture toughness specimen before and after testing can be seen in Figures 5 and 6. Results of the tests are shown in Table 3. Again, the results indicate that the two examined RV control rings are equivalent, even though tensile strength coupons tests performed at Hemet Casting Company suggest otherwise. The average fracture toughness of all tests was 15.05 ksi $\sqrt{\text{in.}}$ (16.6 MPa. $\sqrt{\text{M}}$).

5. Critical Flaw Size Analysis

The critical flaw size of any component is primarily dependent upon three factors: (a) operating stress, (b) the component materials fracture toughness, K_{IC} , and (c) section thickness. In the case of the RV control ring, the maximum operating stress has been demonstrated to be 8.9 ksi (61.4 MPa), occurring at the inner flange section of the RV ring [1]. The fracture toughness of the RV control ring (A356-T6 aluminum) has been shown to be 15.05 ksi $\sqrt{\text{in.}}$ (16.6 MPa. $\sqrt{\text{M}}$). Since primarily surface type casting flaws were found in the low elongation tensile bars from Hemet Casting Company (see paragraph III.E.2), a fracture mechanics solution for a surface flaw loaded in tension [3] was used to calculate the critical flaw size. Therefore,

$$K_I = 1.1 \frac{\sigma}{\sqrt{a}} \sqrt{a/Q}$$

where, $\frac{\sigma}{\sqrt{a}}$ = Operating Stress
 a = Crack Depth
 Q = Flaw Shape Parameter *

* Assume $Q = 1.45$ for $a/2c = 0.250$ and $\sigma/\sigma_{ys} = 0.30$.
($2c$ = crack length) [3].

Applying this solution to the RV control ring;

$$15.05 \text{ ksi } \sqrt{\text{in.}} = 1.1 (8.9 \text{ ksi}) \sqrt{a/1.45}$$

$$1.54 \sqrt{\text{in.}} = \sqrt{a/1.45}$$

$$1.09 \text{ in.} = a ; 2c = 4.36 \text{ in.}$$

Thus, a surface flaw 1.09 in. (27.7 mm) deep and 4.36 in. (110.7 mm) long would have to be present to cause fracture of the RV control ring. This flaw size is considered to be conservative since: (1) the operating temperature at maximum stress (reentry) is approximately 300 °F (149 °C), and (2) plane stress conditions (not plain strain) will primarily influence fracture behavior. For plane strain conditions to exist, the calculated minimum required section thickness would be 0.531 in. (13.5 mm), [4]. The nominal thickness of the

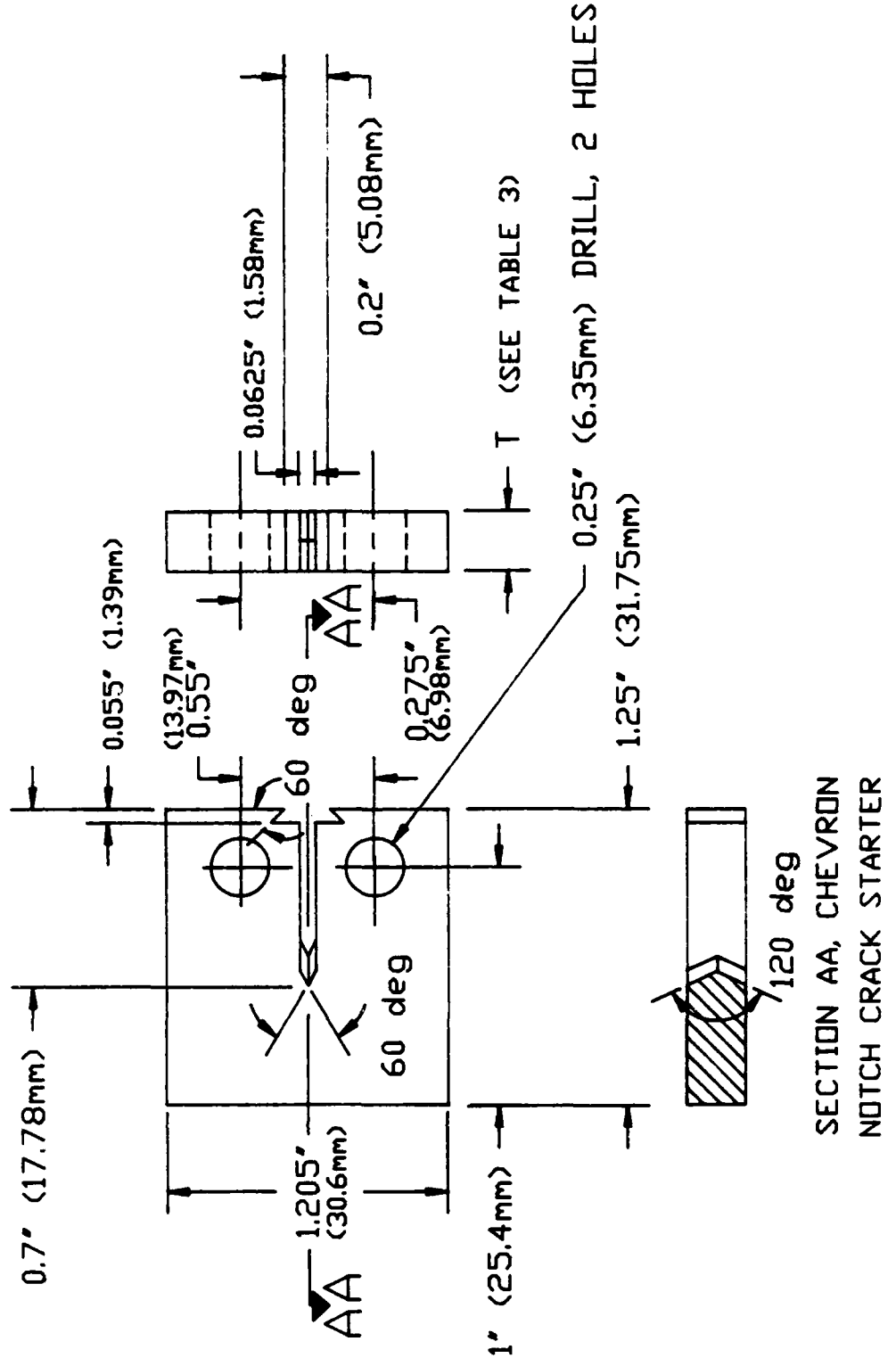


Figure 4. Fracture toughness specimen.

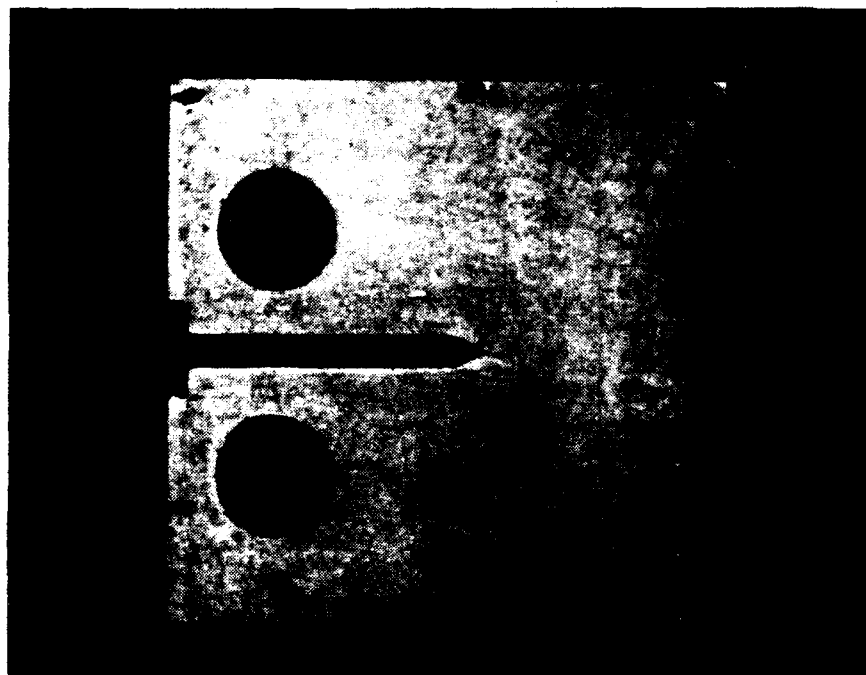


Figure 5. Typical fracture toughness specimen used in this analysis (2.5X).

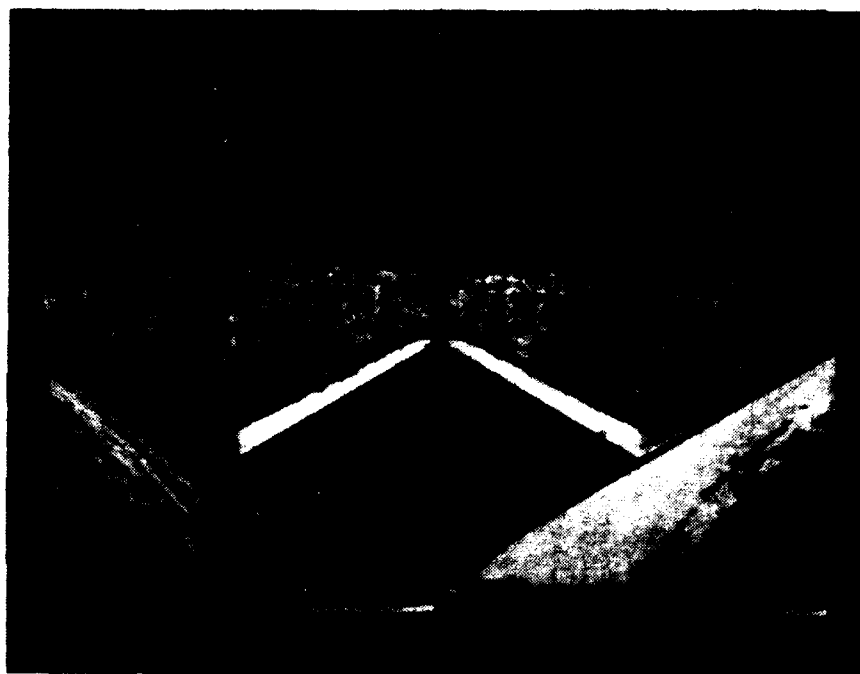


Figure 6. Photograph of fracture surface of typical fracture toughness specimen. Note fatigue pre-crack zone (1) and flat, fast fracture zone (2) (1.1X).

TABLE 3. Fracture Toughness Tests.

RV CONTROL RING SN 10253

Sample	SPECIMEN THICKNESS, in. (mm)	K _{IC} , KSI . $\sqrt{\text{in.}}$ (MPa . $\sqrt{\text{m}}$)
1	1.000 (25.4)	15.3 (16.8)
2	0.916 (23.3)	15.5 (17.0)
3	0.945 (24.0)	14.5 (16.0)
4	0.956 (24.3)	14.7 (16.2)
5	1.001 (25.4)	14.6 (16.1)
6	0.950 (24.1)	15.1 (16.6)
Average K _{IC} =		15.0 (16.5)

RV CONTROL RING SN 60428

Sample	SPECIMEN THICKNESS, in. (mm)	K _{IC} , KSI . $\sqrt{\text{in.}}$ (MPa . $\sqrt{\text{m}}$)
1	0.905 (23.0)	14.5 (16.0)
2	0.904 (23.0)	15.4 (16.9)
3	0.902 (22.9)	14.5 (16.0)
4	0.904 (23.0)	17.4 (19.1)
5	0.902 (22.9)	14.8 (16.3)
6	0.897 (22.8)	15.6 (17.2)
7	0.905 (23.0)	13.8 (15.2)
8	0.888 (22.6)	14.8 (16.3)
Average K _{IC} =		15.1 (16.6)

Test Procedure per ASTM E 399

Loading Rate = 75 KSI . $\sqrt{\text{in./min}}$ (517.1 MPa . $\sqrt{\text{m/min}}$)

Nominal Fatigue Pre-crack = 0.525 in. (13.3 mm)

Material: A356-T6 Aluminum

inner flange wall is 0.120 in. (3.05 mm). Since required radiographic inspection [5] of the RV control ring can detect flaws as small as 0.10 in. (2.54 mm), it is very unlikely that a critical size flaw would be present in any RV control rings.

B. Microstructural Examination - RV Control Rings

Microstructural examination was performed on the web section and jet vane port sections of both RV control rings, Figure 2. A common A356-T6 aluminum microstructure consisting of a eutectic silicon phase in an aluminum matrix was found in both RV control rings. However, the thinner web sections had finer, less angular eutectic silicon particles than did the thicker jet vane port sections as shown in Figures 7 and 8. It is believed that this is caused by different solidification rates which these sections experienced during cooling from the initial pouring of the casting. Thus, the thinner sections cool faster resulting in a finer network of eutectic silicon particles.

Hardness testing was performed using standard Rockwell hardness test equipment. Hardness data was very similar for both RV control rings; both castings had a hardness range of HRF 83-87. Additionally, the measured conductivity for these RV rings ranged from 38-39 percent IACS, indicating the required T6 temper for this alloy.

C. Fractography - RV Control Rings

Fractographic examination of tensile samples and fracture toughness samples was performed using a scanning electron microscope. The fracture features of tensile overload and fatigue for these A356-T6 samples were very similar, Figures 9 and 10. In both tensile overload and fatigue, it is believed that crack growth aligns itself with the brittle eutectic silicon phase following the cast dendritic networks in the microstructure. This would offer fatigue crack growth and tensile overload fracture the least path of resistance, resulting in very similar fracture features. Only in a few isolated areas of the fatigue zone was there clear evidence of fatigue striations, Figure 11. Fractographic examination of samples from the two RV control rings yielded no significant differences.

D. Chemical Analysis - RV Control Rings

The RV control rings are required to be fabricated from A356 aluminum casting alloy per MIL-A-21180. Chemical composition of both RV control rings was determined by emission spectrograph and x-ray fluorescence methods. No chemical composition anomalies were noted in either RV ring. Results of the chemical analysis are shown in Table 4.



Figure 7. Typical microstructure found in the jet vane port section of each RV control ring. Note the size and shape of the eutectic silicon phase. Keller's ETCH (100X).



Figure 8. Typical microstructure found in the web section of each RV control ring. Compare with Figure 7 (100X).

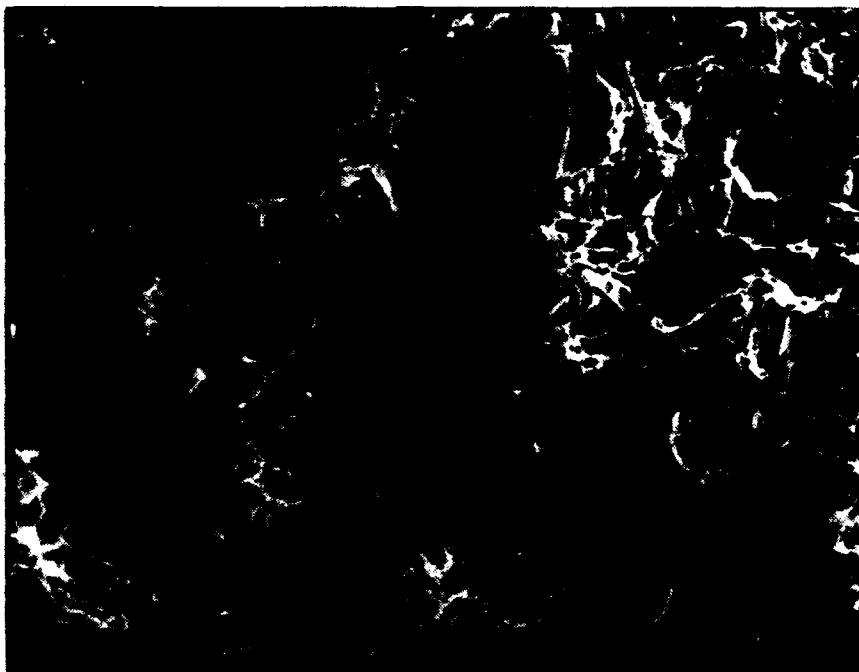


Figure 9. Typical fracture morphology in fatigue zone of fracture toughness samples. Fatigue cracking has occurred along favorably oriented eutectic silicon particles (100X).

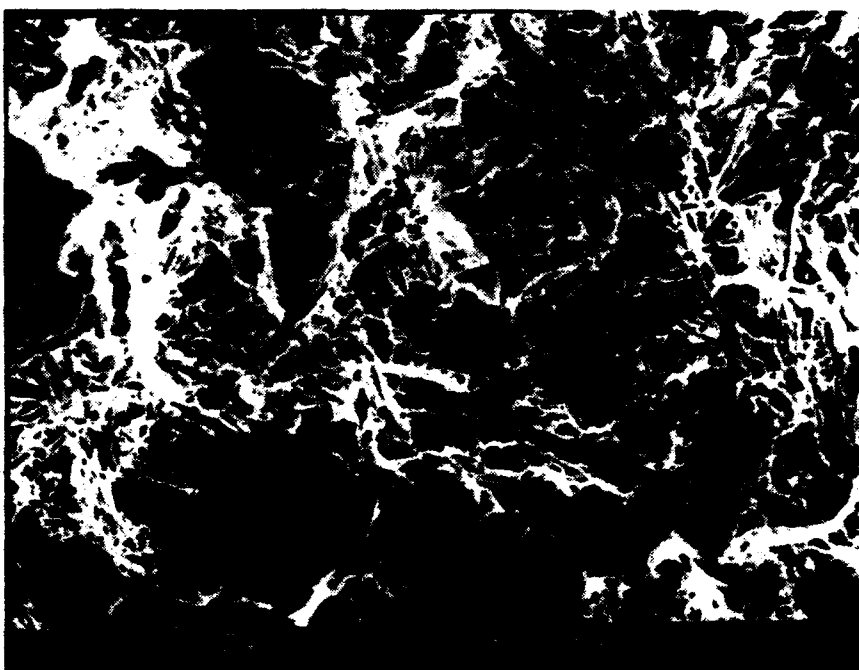


Figure 10. Typical fracture morphology of tensile overload. This was found in tensile test samples and the fast fracture zone of fracture toughness specimens. Compare with Figure 9 (100X).

TABLE 4. Chemical Analysis RV Control Rings.

Element	Ring SN 10253	Ring SN 60428	MIL-A-21180
Silicon, %	6.85	7.0	6.5 - 7.5
Magnesium, %	0.28	0.30	0.25 - 0.45
Iron, %	0.04	0.03	0.20 Max
Copper, %	< 0.2	< 0.2	0.20 Max
Zinc, %	< 0.1	< 0.1	0.10 Max
Manganese %	< 0.1	< 0.1	0.10 Max
Aluminum, %	balance	balance	balance

E. Analysis of Hemet Tensile Coupons

At this point, it is obvious that the two examined RV control rings are equivalent with respect to tensile properties, percent elongation, fracture toughness, chemical composition, and microstructure. Though the Hemet tensile coupon test for RV control ring SN 10253 resulted in tensile properties of 33.7 ksi (232 MPa) ultimate, 29.3 ksi (202 MPa) yield, and 2.5 percent elongation, tensile samples cut from the actual casting resulted in the average tensile properties of 36.9 ksi (254 MPa) ultimate, 31.9 (220 MPa) yield, and 5.4 percent elongation. To determine the major cause of this anomaly, an analysis was performed on 179 broken Hemet Casting Company tensile coupons which had been used for mechanical property determination of RV control rings. All tensile coupons had a gage length of 1 inch.

1. Classification of Hemet Test Coupons

All tensile coupons were classified according to the measured percent elongation. This was done by using the standard procedure of mating the tensile break surfaces together and measuring the elongation between the gage marks. After this was done, 40 samples were selected to represent two groups (20 per group): Group 1 had less than 5 percent measured elongation, and Group 2 had 5 percent or greater measured percent elongation. Of the 179 tensile coupons, 34 tensile coupons had less than 5 percent elongation, with 9 of these 34 having less than 2.5 percent elongation. All 9 tensile coupons with less than 2.5 percent elongation were included in Group 1. All other samples for Group 1 and Group 2 were randomly selected. Fractography, metallography, and chemical analysis were performed to characterize the fracture features, microstructures, and chemical composition of these tensile coupons.

2. Fractography of Hemet Test Coupons

Fractographic examination of the 40 tensile breaks revealed a distinct difference in the fracture features between the two groups of samples. In Group 1, sixteen of twenty tensile breaks had smooth, irregular fracture areas which are believed to be casting flaws (Figures 12, 13, and 14). As shown in Figures 12 and 13, these casting flaws tend to locate themselves on the outer perimeter of the sample though several areas were found where they were located well within the sample midsection. Using a polar planimeter, the percentage of surface area of these casting flaws were measured from the fractographs of the sixteen samples of Group 1. This percentage of surface area flaw ranged from 2.72 percent to 30 percent of the total fracture surface. In two Group 1 samples, casting flaws composed 30 percent of the total fracture surface area of each sample. The measured elongations for these same two samples were 0.8 percent and 1.1 percent.

In contrast, Group 2 had no evidence of these casting flaws on the fracture surface. Omitting the casting flaws, the fracture features of Group 1 and Group 2 were similar, though a more coarse fracture morphology was generally found in Group 1 specimens (Figures 15 and 16). A normal amount of microporosity was found in all samples in both groups (Figure 17).

3. Metallography of Hemet Test Coupons

Microstructural analysis was performed on Group 1 samples having the observed casting flaws on the fracture surface. A very dense and localized segregation of the eutectic silicon phase was found in most samples (Figures 18 and 19). Such a dense concentration of eutectic silicon in a very localized area of the tensile coupon will result in poor mechanical properties, in particular, elongation. Crack propagation during fracture in A356-T6 aluminum will primarily follow the brittle eutectic silicon particles. Therefore, the greater the segregation of eutectic silicon, the more likely brittle fracture will occur as a result of lower mechanical properties.

No areas of localized segregated eutectic silicon were found in any samples of Group 2. However, some samples in Group 2 did display a lesser breakup and spheroidization of eutectic silicon than would be desired for optimum mechanical properties (Figure 20). Better mechanical properties and ductility will normally be obtained if the eutectic silicon phase is broken into smaller particles, i.e., spheroidized. This is accomplished by an adequate solution heat treatment, i.e., by using the proper temperature and time. Note the degree of spheroidized eutectic silicon phase found in a 10 percent elongation sample (Figure 21). Though other factors such as chemical impurities may influence spheroidization, proper solution heat treatment is usually the most important.

Noting the degree of segregated eutectic silicon found in Group 1, proper solution heat treatment would probably not correct this problem since the local density of the eutectic silicon is so high, and the eutectic silicon is already somewhat spheroidized. It is believed this problem was caused by an inadequate casting practice such as inadequate mix of alloys, slow solidification rate, or poor melting and pouring techniques.



Figure 11. Stairstep type fatigue striations found in fatigue zone of fracture toughness specimen (620X).



Figure 12. Macrograph of tensile coupon fracture showing extensive casting flaws (11.5X).

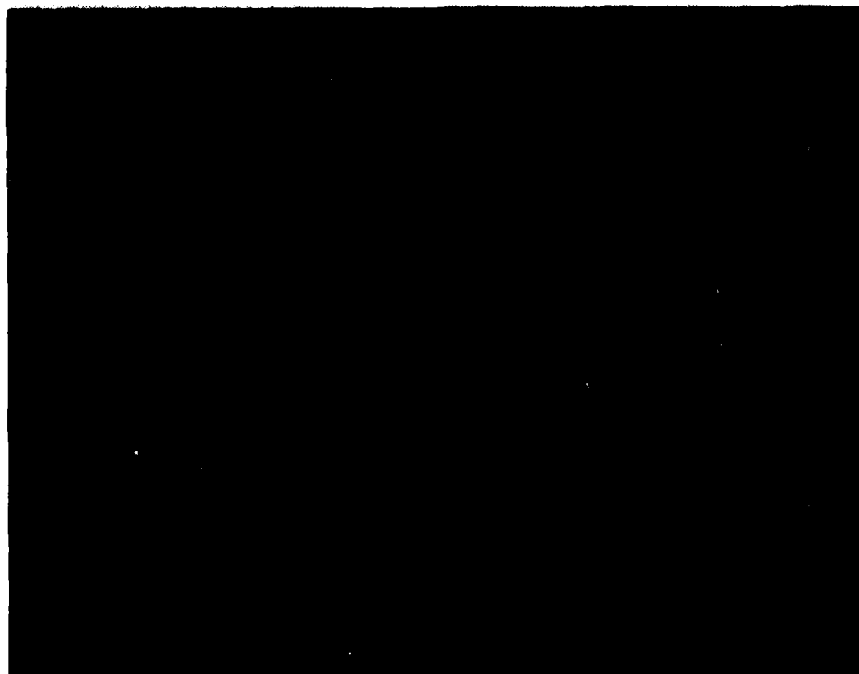


Figure 13. Scanning electron micrograph of typical casting flaws.
Note the distinct irregular appearance (28X).



Figure 14. High magnification SEM photograph of casting flaw
showing uneven ridges which are believed to be
the tips of dendrite tree networks (500X).



Figure 15. Typical Group 1 fracture surface away from casting flaws. Compare with Figure 16 (300X).

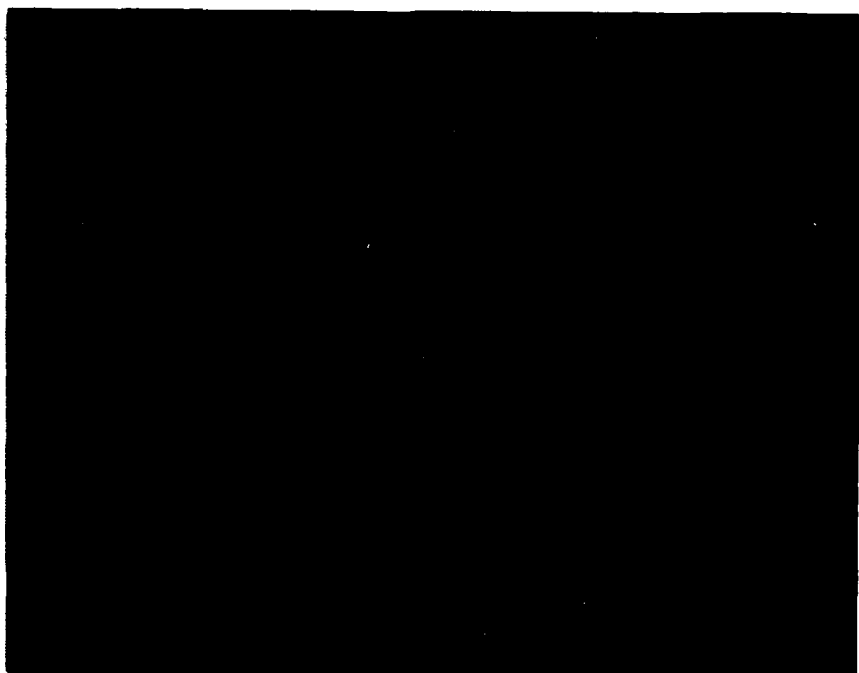


Figure 16. Typical Group 2 fracture surface. Fracture morphology is generally less coarse than that in Group 1 (300X).

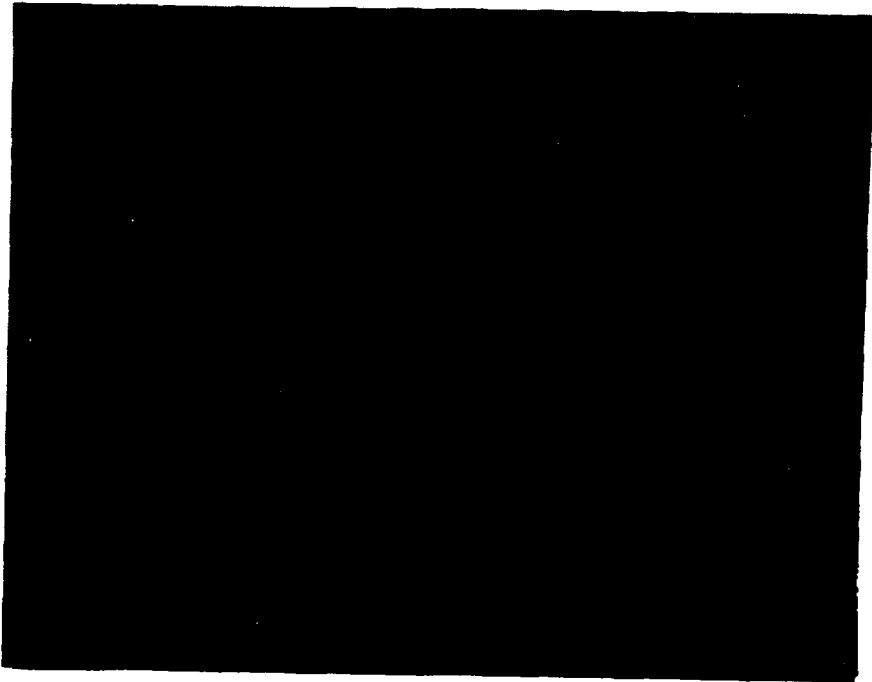


Figure 17. Typical microporosity which was found in all examined samples of Group 1 and Group 2 (100X).



Figure 18. Polished and etched cross section of a Group 1 tensile coupon. Note the dense network of eutectic silicon and dendrites at the break.



Figure 19. Magnified view of Figure 18 showing fracture occurring along the network of segregated eutectic silicon (35X).



Figure 20. Microstructure of Group 2 tensile coupon having 6 percent elongation. Compare to Figure 21 (100X).

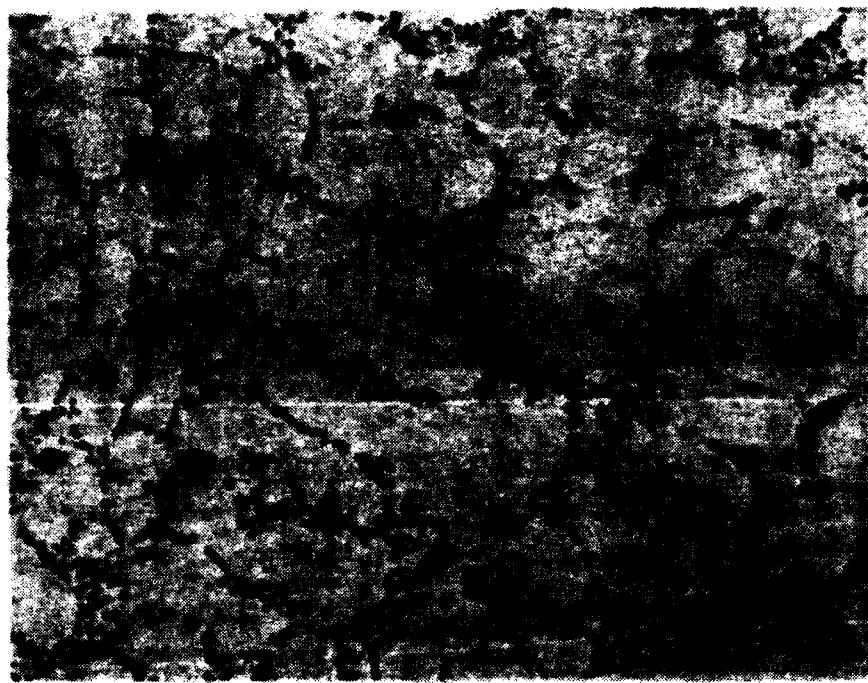


Figure 21. Microstructure of Group 2 tensile coupon with 10 percent elongation. Compare to Figure 20 (100X).

4. Chemical Analysis - Hemet Test Coupons

Chemical analysis of the tensile coupons in Group 1 and Group 2 was performed using emission spectrograph and x-ray florescence methods. No chemical composition anomalies were found. Results are shown in Table 5.

TABLE 5. Chemical Analysis RV Control Rings.

Element	Group 1	Group 2	MIL-A-21180
Silicon, %	6.95	6.87	6.5 - 7.5
Magnesium, %	0.30	0.28	0.25 - 0.45
Aluminum *	balance	balance	balance

* Note: All other chemical composition requirements of MIL-A-21180 were satisfied.

IV. CONCLUSIONS

The following conclusions are drawn from this analysis:

A. The fracture toughness of A356-T6 aluminium used in RV control rings is 15.05 ksi $\sqrt{\text{in.}}$ (16.6 MPa. $\sqrt{\text{m.}}$).

B. RV control rings SN 10253 and SN 60428 have equivalent mechanical properties, fracture toughness, microstructure, chemistry, and elongation. The reported elongation and tensile property data from Hemet Casting Company for RV ring SN 10253 is erroneous.

C. Casting flaws (eutectic silicon segregation) are believed to be the major cause of low percent elongation found in Hemet tensile test coupons.

D. It is likely that casting flaws within Hemet tensile coupons have caused inaccurate (low) mechanical property characterization of RV control rings.

E. Ductility, as measured by percent elongation, is an important material characteristic and should not be ignored. It has proven to indicate the existence of brittle casting flaws in tensile coupons.

V. RECOMMENDATIONS

The following recommendations are made regarding the RV control rings:

A. Hemet Casting Company should insure that future cast tensile coupons represent the true properties of the RV control rings.

B. It is strongly recommended that future RV control rings, as well as all other PII casting components, having reported below specification elongation or tensile/yield strength properties, be disqualified and replaced, by the contractor, with components having proper mechanical properties.

REFERENCES

1. "Investigation of the PII RV Control Ring Casting as Produced by HEMET Casting Co." Document No. ANA 10722080-001, Martin Marietta Corporation, Orlando, FL.
2. Roark, Raymond J., and Young, Warren C., Formulas for Stress and Strain, Fifth Edition, p. 594.
3. Fracture Mechanics Design Handbook, U.S. Army Missile Research and Development Command, Redstone Arsenal, AL, Technical Report TL-77-8. p. 194.
4. Standard Test Method for Plane - Strain Fracture Toughness of Metallic Materials, ASTM E 399, p. 9.1.3
5. Military Specification, MIL-A-21180C, Grade C, Size 2 shrinkage cavity, 15 January 1964, p. 4.

DISTRIBUTION

	<u>No. of Copies</u>
Martin Marietta Aerospace ATTN: Ron Gast P.O. Box 5837 Mail Point 246 Orlando, FL 32855	6
IIT Research Institute ATTN: GACIAC 10. W. 35th Street Chicago, IL 60616	1
U.S. Army Materiel System Analysis Activity ATTN: AMXSY-MP Aberdeen Proving Ground, MD 21005	1
AMSMI-RD, Dr. McCorkle	1
Dr. Rhoades	1
-RD-ST, Dr. Mixon	1
Mr. Letson	1
-RD-ST-CM, Mr. Howard	1
Mr. Austin	1
Mr. Parker	1
Mr. Ingram	1
Mr. Goodwin	12
Ms. Watson	1
-RD-ST-SA, Mr. Christensen	1
Dr. Smith	1
Mr. Patrick	1
-RD-PR, Dr. Stephens	1
-RD-PR-M, Mr. Crownover	1
Mr. Wright	1
-RD-CS-R	15
-RD-CS-T	1
AMSMI-GC-IP, Mr. Bush	1
AMCPM-PE, Mr. Noller	1
Mr. Switzer	1